Solar Energy Materials and Solar Cells 190 (2019) 30–36

Contents lists available at ScienceDirect

Solar Energy Materials and Solar Cells

journal homepage: www.elsevier.com/locate/solmat

Optimization of phosphorus dopant profile of industrial p-type mono PERC solar cells

Feng Ye[a,b], Yunpeng Li[a,b], Xuguang Jia[a], Huafei Guo[a], Xiuqin Wang[a], Jianning Ding[a,c,**], Ningyi Yuan[a,*], Zhiqiang Feng[a,b]

[a] Jiangsu Collaborative Innovation Center of Photovoltaic Science and Engineering, and the Breeding Construction Point of State Key Laboratory of Photovoltaic Engineering Science, Changzhou University, Changzhou 213164, China
[b] State Key Lab of PV Science and Technology, Trina Solar, Changzhou 213031, China
[c] Micro/Nano Science & Technology Center, Jiangsu University, Zhenjiang 212013, China

ARTICLE INFO

Keywords:
PERC solar cell
Emitter profile
Saturation current density J_0
Contact resistance

ABSTRACT

Passivated emitter and rear cells (PERC) on p-type Cz Si wafers are currently being migrated to mainstream production, applying the ongoing improvements in recent years. For PERC solar cells, the emitter recombination loss becomes the main loss of the entire cell. Currently, two-step diffusion consisting of low temperature phosphosilicate glass (PSG) deposition and high-temperature drive-in has been widely applied in production and can reduce saturation current density (J_0) of the emitter in the passivated area. However, a low contact resistance under metal area cannot be guaranteed. Meanwhile, the determination of the saturation current density J_0 in the passivated area is dependent on the injection density during the measurement, and exact calculation of $J_{0,\mathrm{metal}}$ is not as convenient as $J_{0,diffusion}$, which could lead to a wrong assessment in cell analysis. In this study, a three-step diffusion (low-temperature PSG deposition–high-temperature drive-in–low temperature PSG deposition) with low J_0 and low Ag-Si contact resistance is investigated and combined with a selective emitter by an etch-back process. The results are compared with a conventional two-step $POCl_3$ diffusion. The accuracy of J_0 measurement and $J_{0,metal}$ test method is also discussed. With these improvements, the champion cell efficiency of our PERC solar cells fabricated on 156 × 156 mm^2 wafers using screen printing technology and industrial-type process has reached 22.61% with Voc of 684.4 mV and a fill factor of 81.49%, as confirmed by Fraunhofer ISE CalLab PV cells. By implementing the diffusion process to mass production, the average cell-efficiency gain is approximately 0.2% with a median efficiency of 21.7%.

1. Introduction

The industrial passivated emitter and rear cell (PERC) capacity is globally 15 GW at present (compared with the 84 GW standard production) and is forecasted to globally expand by approximately 10 GW in 2017 [1,2]. By 2020, 61 GW of PERC production (compared with the 77 GW standard) may be achieved. The advantage of PERC cells, higher efficiency, must be greater than their disadvantage, higher manufacturing costs. In recent years, selective emitter (SE) solar cells have been commercially mass-produced. For SE solar cells, the main advantages are as follows: 1) increase of quantum efficiency at short wavelength, 2) decrease of contact resistance R_c, and 3) decrease of emitter saturation current density J_{0e}. These improvements result in an improvement in the open-circuit voltage (Voc), short-circuit current (I_{sc}), and fill factor (FF) [3]. The techniques for SE formation have been intensively researched, and many methods can be used for mass production [4–8]. Laser-doped SE [9] has begun to be applied in mass production owing to its lower operating cost. However, the mask and etch process using inkjet printing of a resist mask and a wet chemical etching process to etch a highly doped surface layer has more potential for cell-efficiency improvement than the laser-doped SE, because J_0 of the highly doped region is lower due to absence of laser damage. Literature values for the J_0 of laser-doped areas report values of about 200 fA/cm^2 after passivation at a sheet resistance of 60 Ω/sq. [10], which is significantly higher than as-diffused emitters.

The universal two-step diffusion contains a low-temperature

* Corresponding author.
** Corresponding author at: Jiangsu Collaborative Innovation Center of Photovoltaic Science and Engineering, and the Breeding Construction Point of State Key Laboratory of Photovolatic Engineering Science, Changzhou University, Changzhou 213164, China.
E-mail addresses: dingjn@cczu.edu.cn (J. Ding), nyyuan@cczu.edu.cn (N. Yuan).

https://doi.org/10.1016/j.solmat.2018.10.002
Received 20 January 2018; Received in revised form 30 September 2018; Accepted 1 October 2018
Available online 26 October 2018
0927-0248/

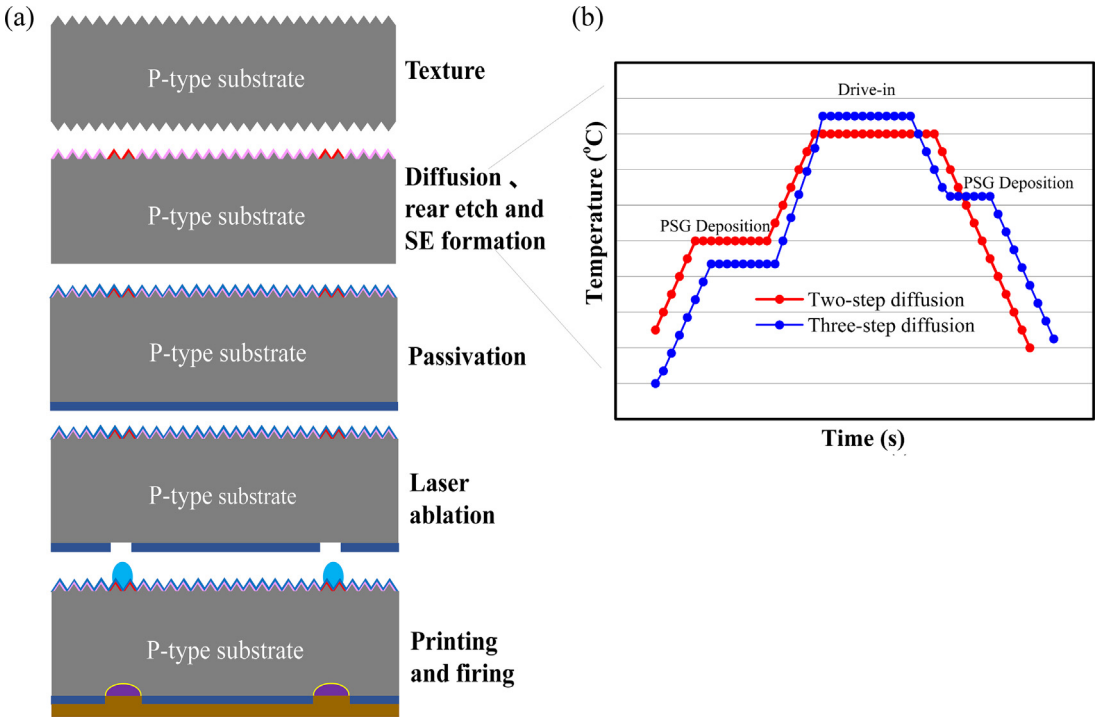

Fig. 1. Process flow of PERC solar cell fabrication (a), and the sketch of two-step and three-step diffusion process (b).

phosphosilicate glass (PSG) deposition and a high-temperature drive-in, which can reduce the surface phosphorus concentration, increase the junction depth, and yield good uniformity of sheet resistance R_{sheet}. Therefore, the surface concentration of the lightly doped area is always below 1×10^{20} cm^{-3} after the etch-back process and $J_{0,light}$ can be reduced to approximately 20–30 fA/cm^2 at a sheet resistance of 140–150 Ω/sq [11]. However, a lower surface phosphorus concentration of the heavy diffusion area will increase the contact recombination and Ag-Si contact resistance R_c [12]. Therefore, even though a high Voc is obtained, the FF will be decreased compared to the normal diffusion process with same PSG deposition and drive-in temperature.

In this paper, to reduce Ag-Si contact resistance R_c under the metal area and keep the low J_0 of the emitter, a three-step diffusion was adopted [13,14]. Fig. 1a and b show the process flow of the PERC solar cell fabrication and a rough sketch of the two- and three-step diffusion processes, respectively. Compared with the two-step diffusion, the three-step diffusion has a lower-temperature PSG deposition, higher-temperature drive-in, and was combined with another low-temperature PSG deposition process after the drive-in step. The last low-temperature PSG deposition process can obtain a high surface phosphorus concentration, which is beneficial to the Ag-Si contact resistance, and a low J_0 of the lightly doped area can be obtained because a narrow high concentration area can be etched using an etch-back process. To optimize the phosphorus dopant profile, the analysis of the saturation current is needed. The J_0 value was affected by the injection densities [15,16], and the J_0 value could be underestimated under a low injection density, which would give a wrong information. Therefore, we used robust statistics to determine the maximal J_0 value under different injection densities. Meanwhile, the recombination loss under a metal area is usually very large and $J_{0,metal}$ measurement is not as convenient as the measurement of J_0 in the diffusion area. A method of four different types of metallization-ratio areas designed on diffused and passivated high-resistivity wafer was used for the $J_{0,metal}$ calculation. Based on the J_0 analysis, the three-step diffusion method balances the relationship between Voc and FF of the cell efficiency better, maintains lower $J_{0,emitter}$, and increases the Ag-Si contact performance. The efficiency of our best mono PERC cells reached 22.61% [17]. Such advanced profiles are continuously advanced to mass production, which currently has a median efficiency of 21.7%, and the cell-efficiency gain is approximately 0.2% compared to the baseline two-step diffusion.

2. Experiment design

P-type 156 × 156 mm^2 monocrystalline Czochralski silicon wafers with a resistivity of 1.6 Ω cm and a thickness of 180 μm were used in the PERC solar cell fabrication. First, the front textured surface was formed by an industrial-type alkaline texturing process. An emitter with a median sheet resistance of approximately 65 Ω/sq measured by four point probe was formed by the phosphorous diffusion. After the diffusion process, the rear PSG layer was removed by single-side diluted hydrofluoric acid (HF) cleaning while the front-side PSG layer was retained. The rear side was then polished using alkaline solution with an industrial wet bench. The front heavily doped emitter was selectively etched by $HF/HNO_3/H_2O$, which was realized using inkjet masking in the finger area. The median sheet resistance of lightly doped area is around 150 Ω/sq. The width of the heavily doped area is 180 μm and the printed finger width is about 50 μm. There is no heavily doped area under the busbars because floating busbars were used. The PSG at the heavily doped area was removed after ink removal. The rear AlO_x/SiN_x stack films and front passivation/antireflection-coating (ARC) SiN_x were deposited by plasma-enhanced chemical vapor deposition. A picosecond laser with a 532 nm wavelength was used to selectively open the passivation film on the rear side of the cell. Ag-Si and Al-Si contacts were formed by screen printing and co-firing in a belt furnace.

The reference process is a two-step diffusion with an emitter sheet resistance of approximately 65 Ω/sq. The optimized process is a three-step diffusion with a sheet resistance of approximately 63 Ω/sq. The relationship between the etching time and sheet resistance after the etch-back process was investigated. The phosphorus doping concentration profiles in the diffused and the etched-back areas were measured on the textured surface using the electrochemical capacitance-voltage (ECV) method, and the curves were applied a correction to the measured sheet resistance.

To measure emitter saturation current density J_{0e}, 156 × 156 mm^2

p-type monocrystalline Czochralski as cut silicon wafers with a bulk resistivity of 10 Ω cm and a thickness of 180 μm were used. The double-side texturing and $POCl_3$ diffusion in both types of the diffusion process were followed by double-side passivation using fired SiN_x. $J_{0,light}$ of lightly doped area was measured once the double-side etch-back was completed, followed by fired SiN_x passivation. The emitter saturation current density was measured using the quasi-steady-state photo conductance (QSSPC) method [18].

3. Results and discussions

3.1. Methods of emitter saturation current density J_{0e} calculation

The saturation current density J_0 of the heavily doped area with a R_{sheet} of 65 Ω/sq and lightly doped area with a R_{sheet} of 150 Ω/sq of the emitter were extracted from lifetime measurements of two different test samples, using a Sinton WCT-120 lifetime tester by applying the method of Kane and Swanson [19] and an intrinsic carrier density $n_i = 8.6 \times 10^9$ cm^{-3}.

The predominant contribution to the improved Voc comes from the low emitter J_0 realized by an advanced passivation technology and an optimized doping profile. However, the J_0 value, extracted from the lifetime curves, depended on the injection density Δn. This dependence became relatively large when low J_0 values were measured. Fig. 2(a) and (b) show the J_0 values of the lightly and heavily doped areas of the two-step diffusion, respectively. We used robust statistics of the 18 samples (five measurements of different areas on each sample) processed in the same batch, i.e., the box spanned the interquartile range (IQR) from 25% to 75%, including the median line, whereas the whiskers were maximally chosen by 1.5 IQR away from the box. In this manner, we could discern outsiders and remove them. From Refs. [15,16], we learned that local Δn at the junctions is lower than average Δn monitored by the lifetime tester, which leads to underestimated J_0 values. The diffusion with large J_0 draws more current to maintain its recombination, and hence, Δn starts decreasing at the junctions relative to the middle at lower injection densities than a diffusion with a small J_0. However, when the carrier diffusion is considered, which is relevant especially for surfaces with higher recombination, the data also converges in high injection [20]. The optimum Δn for J_0 extraction approaches its maximum value, which, therefore, is above 7×10^{15} cm^{-3} for the lowest J_0 value of light diffusion and of the heavy diffusion. Hence, we extract J_0 = 25.5 and 114 fA/cm^2, respectively. Simulating the measurement with the device simulator Sentaurus (blue line) reveals that even at the maximum J_0 value, the local Δn at the junctions remained slightly lower than the average Δn; thus, the actual J_0 of the lightly diffused emitter was slightly higher at 26.3 fA/cm^2. If J_0 had been extracted below 7×10^{15} cm^{-3}, as is often done in literature, it would have been significantly underestimated by more than 10% (the typical uncertainty of J_0 measurements). In that case, reproduction by numerical simulations would necessitate determining surface recombination velocity values that are significantly low and would imply that no room is available for improvement. Hence, to realistically assess the surface passivation quality of good emitters, the precision of the J_0 measurements must be improved, as performed in this study.

The recombination loss under a metal area is usually very large and difficult to represent. Thus, understanding how to measure $J_{0,metal}$ is very important for cell analysis. The high-resistivity wafers were first textured and diffused with a sheet resistance of approximately 65 Ω/sq, then passivated at both sides. Four different types of metallization-ratio areas (A, B, C, D) were designed on the single side of the sample, [see Fig. 3(a)]. From areas A to D, the contact fraction ratio decreased with increasing finger gap. After the Ag paste was removed by aqua regia ($HCl:HNO_3$ = 3:1), $J_{0,total}$ of these four areas were measured using the QSSPC method. The following equation was applied to calculate $J_{0,metal}$ from various $J_{0,total}$ measurements:

$$J_{0,total} = J_{0,metal} \times f + J_{0,diffusion} \times (1 - f) + J_{0,diffusion}, \quad (1)$$

$J_{0,diffusion}$ denotes the saturation current of diffusion for the passivation film only after firing, and it can be measured by the symmetrical structure. The contact fraction f can be calculated by the finger width and finger space. In order to eliminate the influence of passivation quality and possible contamination problems, photoluminescence (PL) of all the samples must be measured to remove the contaminated wafers. Otherwise $J_{0,total}$ would be affected by the contaminated area, and $J_{0,metal}$ will not be accurate, which was calculated via $J_{0,total}$. $J_{0,total}$ denotes the saturation current of these four areas, and with decreasing contact fraction f, $J_{0,total}$ decreases, [see Fig. 3(b), where the cross section of the sample is also shown]. A linear fit of $J_{0,total}$ with different contact fraction f can be carried out using the following equation:

$$J_{0,total} = (J_{0,metal} - J_{0,diffusion}) \times f + 2J_{0,diffusion}, \quad (2)$$

The slope ($J_{0,metal}$ - $J_{0,diffusion}$) and intercept ($2J_{0,diffusion}$) can be received by this linear fit, so $J_{0,metal}$ could be calculated by this method.

3.2. The two-step diffusion

Emitters made by phosphorus diffusion consist of two distinct layers: a so-called kink layer close to the surface, and a slightly doped tail layer underneath, [see Fig. 4(a), as-diffused profiles of the two-step diffusion measured using ECV method on textured surface]. With increasing R_{sheet}, the peak phosphorus concentration decreases and the kink layer narrows down. Bentzen et al. highlighted the unique feature of phosphorus diffusion into silicon [21], that the boundary of the kink and the tail layers always appears where the phosphorus concentration

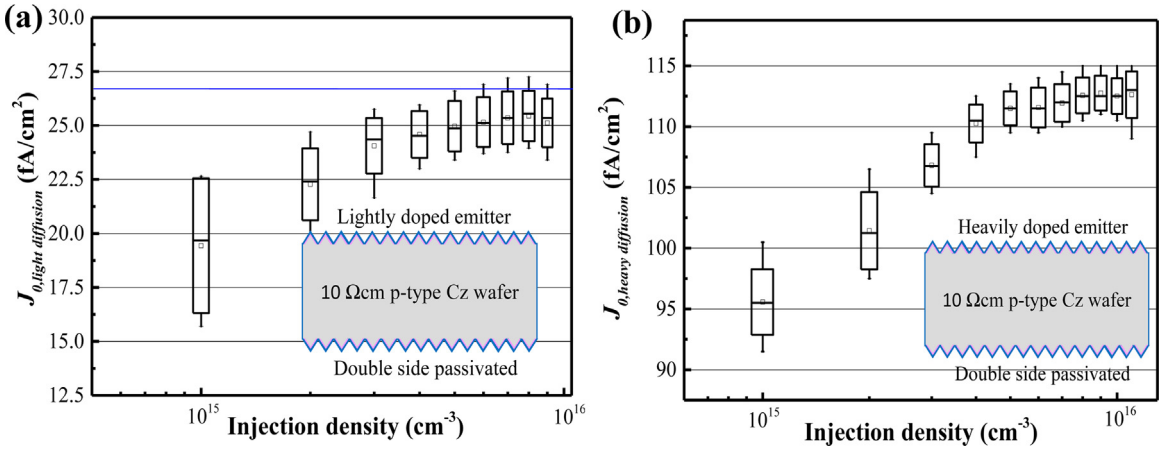

Fig. 2. J0 of the lightly doped area (a), heavily doped area (b) of two-step diffusion process under different injection density and the cross section of monitor sample.

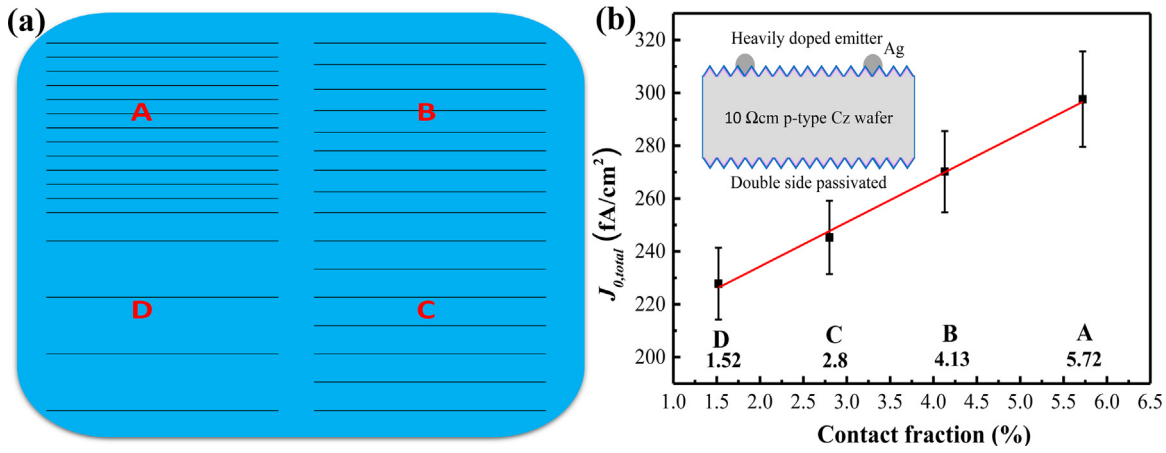

Fig. 3. The sketch of J0, metal monitor sample (a), J0,total of different contact fraction and the cross section of monitor sample (b).

is about 3×10^{19} cm^{-3}. The increase in R_{sheet} contributes to the improvement in both Voc and I_{sc} by reducing saturation current density J_0. Especially in the kink layer where the concentration is 1×10^{20} cm^{-3}, the bandgap-narrowing effect is significant [22], and the effect of Auger recombination is too large to be ignored [23]. The excess phosphorus at more than 5×10^{20} cm^{-3} is electrically inactive [24], causing Shockley–Read–Hall (SRH) recombination [25]. Our previous work [11] focused on reducing these SRH recombination centers by decreasing the peak phosphorus diffusion from 1×10^{21} cm^{-3} to 5×10^{20} cm^{-3} while keeping R_{sheet} at 60–70 Ω/sq, which resulted in a 0.1–0.2% absolute efficiency gain. However, a lower peak phosphorus concentration could cause another problem such as contact resistivity issues, i.e., limiting further improvement in the cell efficiency.

Fig. 4(b) shows the trends of $J_{0,diffusion}$ and $J_{0,metal}$ under different R_{sheet} values for the two-step diffusion on homogeneous emitters. Each point represents one sample corresponding to $J_{0,diffusion}$ and $J_{0,metal}$. The variation in R_{sheet} was obtained by varying deposition parameters such as $POCl_3$:O_2 flow, deposition temperature, and time. With the increase in R_{sheet}, $J_{0,diffuison}$ decreases due to the decreasing peak phosphorus concentration and narrowing kink layer. However, $J_{0,metal}$ increases

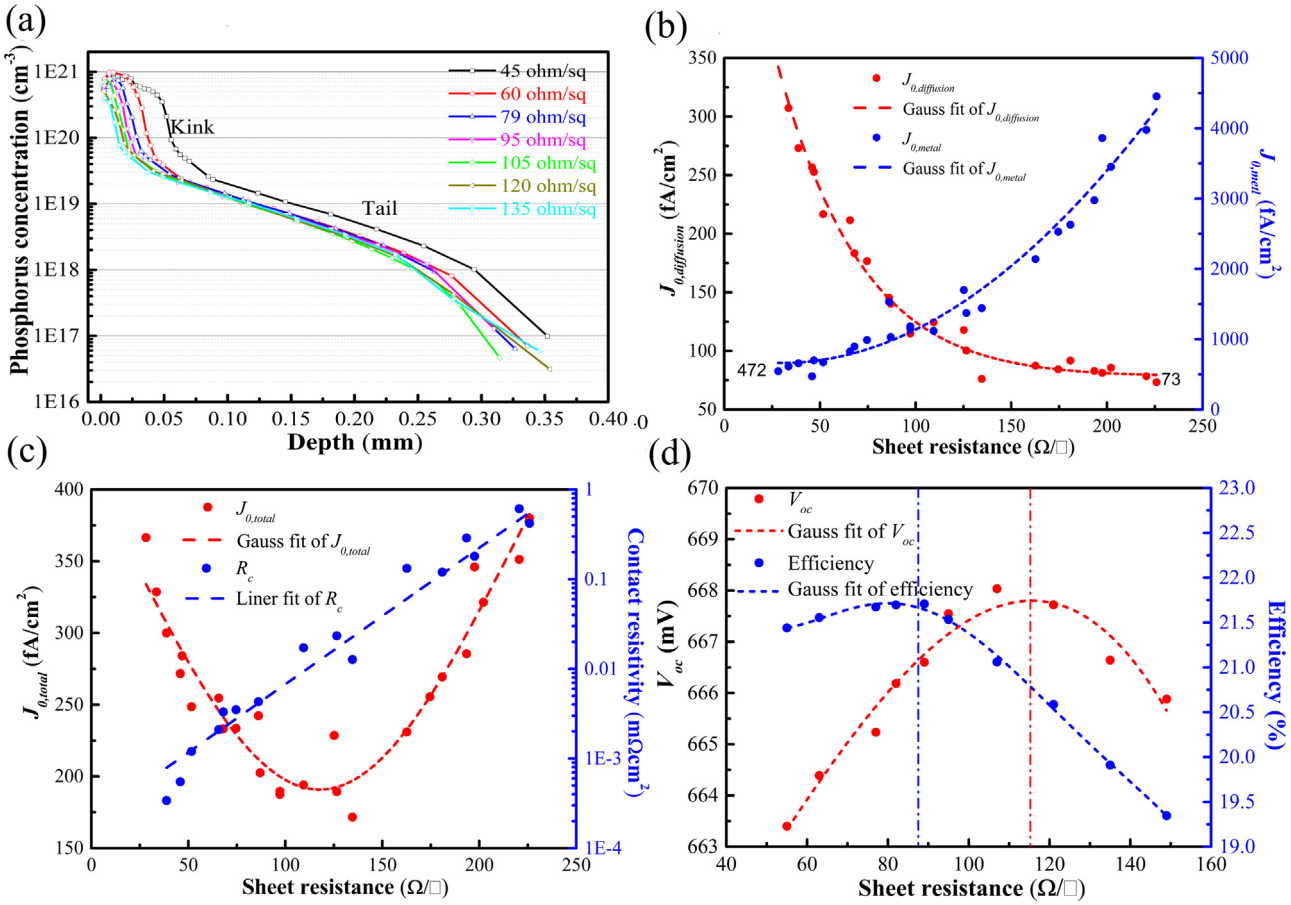

Fig. 4. The dopant profiles under different sheet resistance Rsheet were measured using ECV method and the curves were applied a correction to the measured sheet resistance. (a), the measured J0, pass and J0, metal under different Rsheet (b), the total J0 and measured contact resistance under different Rsheet (c), the simulated Voc and efficiency under different Rsheet (d).

with increasing R_{sheet}, which was caused by the reduced surface doping level and depth of increased R_{sheet}. By considering the fraction of each part, $J_{0,total}$ under different R_{sheet} values can be obtained. Fig. 4(c) shows that the lowest $J_{0,total}$ value is below 110 Ω/sq, and the measured contact resistivity R_c using the transfer length method (TLM) has an exponential relationship with R_{sheet}. The cell efficiency can be simulated using the device simulator Sentaurus. The measured R_{sheet}, R_c, dopant profile, bulk lifetime, surface recombination velocity, and so on are needed to be input for simulation. Therefore, we can see that R_{sheet} of maximum Voc is higher than that for the maximum efficiency because of contact resistivity R_c [see Fig. 4(d)]. Therefore, we need to optimize the dopant profile to have a higher concentration for better contact resistivity and a narrow kink layer that can be etched for a lower saturation current of the lightly doped area, i.e., *the three-step diffusion.*

3.3. The three-step diffusion

To obtain this doping profile, a three-step diffusion process was researched and compared with the two-step diffusion process. This three-step diffusion was the two-step diffusion combined with another low-temperature PSG deposition process after the drive-in step, and other parameters such as $POCl_3/O_2$ ratio were also optimized. Fig. 5(a) shows the dopant profiles of the heavy (as diffused) and light (etch-back) areas of these two diffusion processes. We can observe that the peak phosphorus concentration of the new diffusion was higher than that of the two-step diffusion. However, the kink area was narrower, and the junction depth was deeper, which could maintain the same R_{sheet} of diffusion. After etch-back, the dopant profiles did not exhibit much difference, but the etching rate for the two diffusion processes was different, [see Fig. 5(b)]. The etching time of three-step diffusion was longer than that of the two-step diffusion for the same etching R_{sheet}, which was caused by the narrower kink area and deeper junction depth. However, the uniformity of R_{sheet} after etching for the three-step diffusion has been improved compared with that of the baseline emitters. The texture surface will be etched about 50 nm after the etching process, and the reflectivity will increase slightly.

Fig. 5(c) shows the J_0 measurements on 22 or 19 lifetime samples using either the lightly or heavily doped passivated emitter part on both textured surfaces. For the heavily doped area, J_0 of the new diffusion process was slightly higher, which was caused by the higher recombination within the highly doped kink area, and the SRH recombination should be higher. For the lightly doped area, J_0 of these two diffusions did not differ too much because the surface phosphorus concentration of the new diffusion is also sufficiently low after etch-back. The narrow kink area would be etched even if it has a high peak phosphorus concentration. $J_{0,metal}$ values of the two-step and three-step diffusion were calculated to approximately 810 and 750 fA/cm^2, respectively. By considering that the fractions of the heavily doped area and metal area are about 10% and 4% of the entire emitter, $J_{0,emitter}$ does not differ significantly for these two diffusion processes.

Contact resistance R_c among the cells with different emitters was compared using the TLM. To ensure good contact between the probe and fingers, the fingers were made approximately 200 μm wide, which is much wider than that in real cells. The results are shown in Fig. 5(d). To compare R_c of the two different emitters, we used a notched box plot [26]. The notch indicates the confidence interval of the median. If the

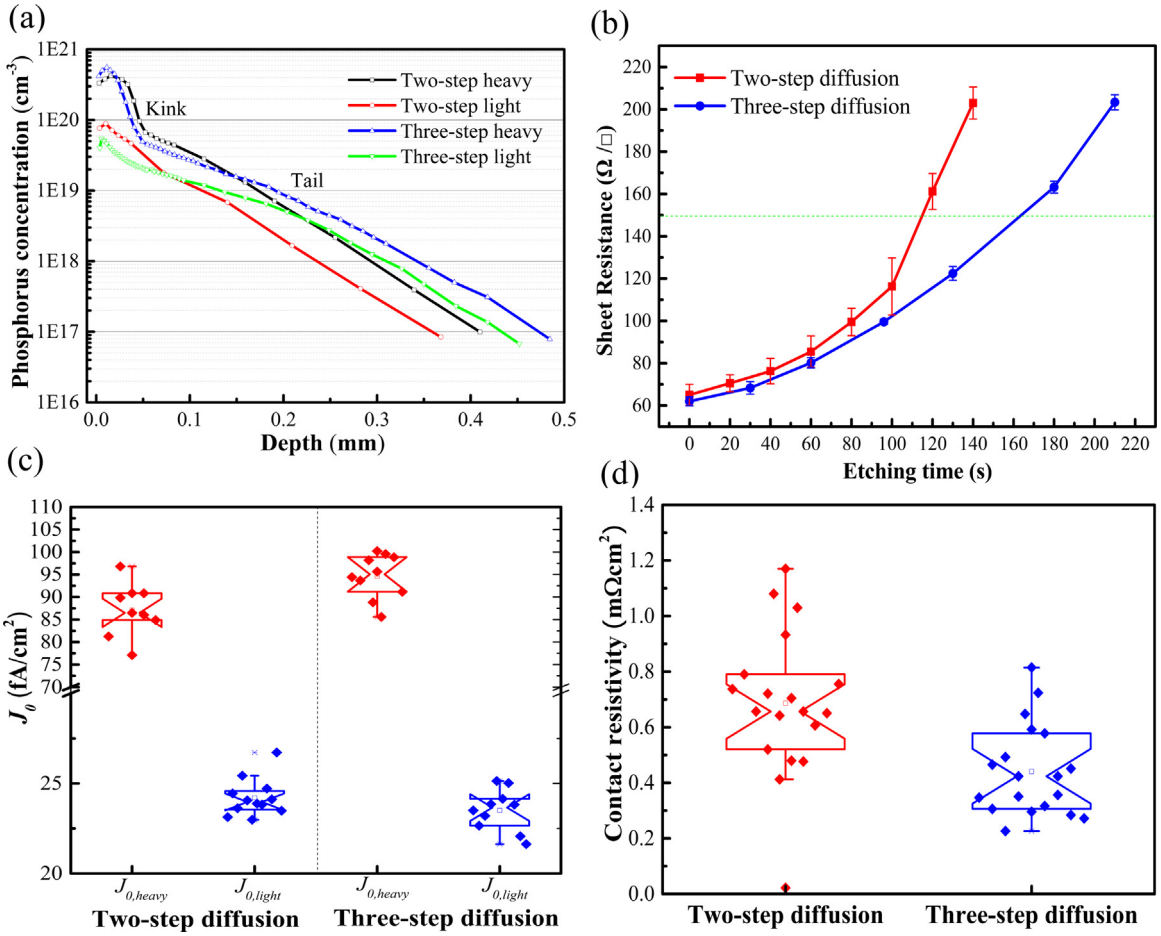

Fig. 5. The heavy (as diffused) and light (etch-back) dopant profiles of two-step and three-step diffusion (a) measured on the textured surface by ECV method which the curves were applied a correction to the measured sheet resistance, etching rate of this two diffusion (b), J0,heavy and J0, light comparison (c) and contact resistance comparison (d).

Table 1
The I-V parameters for the cells with different emitter profile.

	V_{oc} (mV)	J_{sc} (mA /cm^2)	*FF* (%)	*Eff* (%)	R_s Ωcm^2	*pFF* (%)
Two-step diffusion	686.6	39.85	80.44	21.99	0.574	83.54
Three-step diffusion	685.7	39.93	80.78	22.12	0.532	83.64

Table 2
The IV parameters of the best PERC cell, measured at calLab, and median values of the batch, measured in-house.

	V_{oc} (mV)	J_{sc} (mA /cm^2)	*FF* (%)	*Eff* (%)	V_{mpp} (mV)	J_{mpp} (mA/ cm^2)	Cell area (cm^2)
Median	683.8	40.46	81.16	22.45	583.57	38.45	243.36
Best cell	684.4	40.54	81.49	22.61	587.9	38.48	243.23

median is obtained from larger number n of measurement points, its confidence interval shrinks according to ± 1.57 IQR/sqrt(n). Hence, the two experiments yielded a statistically significant difference only in the median when the two notches did not overlap. Therefore, the newly developed emitter profile allows for a reduced R_c. We note that the notched box plots can also be used to determine the minimal number of samples which is necessary to draw relevant conclusions about the two experiments. The smaller the expected difference in the median is, the larger is the number of samples.

Subsequently, PERC cells were fabricated to compare the *I-V* performance of the different emitter profiles, as listed in Table I. A statistically significant improvement in the fill factor was realized, which was consistent with the contact resistance measurements on the cells with different emitter profiles, and the pFF of the three-step diffusion was also higher, which could be caused by the better lightly doped area and metal contact area. In fact, Voc of the three-step diffusion should be a little higher, while the slight decrease in Voc was probably caused by process control or some other influence. Then, this new emitter profile was used in our champion PERC solar cell. Moreover, the triple layer ARC, a better Ag-Si contact and plasticity Ag paste, and a better rear local back surface field (LBSF) were used on our champion PERC solar cell.

The *I-V* performance of the champion cell was measured at Fraunhofer ISE CalLab PV cells, and the result is listed in Table 2. Fig. 6(a) shows the *I-V* curve of the champion PERC solar cells independently measured by Fraunhofer ISE CalLab PV cells. We repeated our in-house measurement of all the cells in the batch with the new calibration using a Sinton FCT-450 flash tester and obtained a median efficiency of 22.45%, as shown in Fig. 6(b). Our measured FF had to be multiplied by 1.002 to match the value obtained by Fraunhofer ISE CalLab PV cells. Fig. 6(b) shows the box plots where the box height spanned from the first to the third quartile IQR, and the whiskers extend maximally by 1.5 IQR. The main improvements from our last champion cell efficiency 22.13% independently measured by Fraunhofer ISE CalLab PV cells [27] are mainly due to a higher FF followed by a higher Voc. The FF increased 1.22%$_{abs}$, and Voc improved by 4 mV. The co-optimization of the phosphorous diffusion profile and the Ag-Si contact as well as better control of the cell process ensures high fill factor and Voc, which are the main contributors to the cell-efficiency promotion. This three-step diffusion is continuously forwarded to mass production, which currently has a median efficiency of 21.7% and a cell-efficiency gain of approximately 0.2%.

4. Conclusions

This study investigated a three-step diffusion process. Robust statistics was used for J_0 value extraction under different injection densities in order to obtain an accurate J_0 value. Four different types of metallization-ratio areas were designed on a high-resistivity wafer for the $J_{0,metal}$ calculation. Compared with the two-step diffusion, this three-step diffusion was based on the two-step diffusion combined with another low-temperature deposition after the drive-in step and other parameters were also optimized. Therefore, it has a high surface phosphorus concentration under the metal area and low J_0 of the lightly doped area because of the narrow kink layer, which could be etched using the etch-back process. In addition, $J_{0,metal}$ under the metal area was reduced by the higher concentration. This three-step diffusion balances the relationship between Voc and FF of the cell efficiency better, maintains lower $J_{0,emitter}$, and increases the Ag-Si contact performance. From this research, the efficiency of our mono PERC cells could be increased to 22.61%. The advanced doping profiles are continuously transferred to mass production, which currently has a median efficiency of 21.7% and a cell-efficiency gain of approximately 0.2% could be achieved.

Acknowledgement

This work was supported by the National Natural Science Foundation of China (Grant No. 51572037, 51335002), Jiangsu Province Key Research and Development Project (BE2017006-3), Jiangsu Province Natural Science Foundation Project (BK20151192),

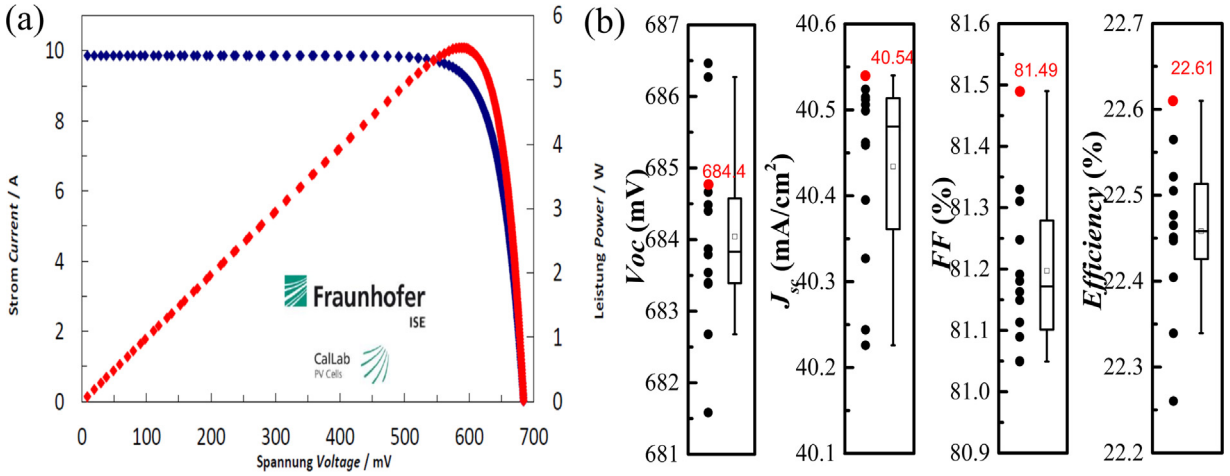

Fig. 6. IV curve of champion PERC solar cells independently measured by Fraunhofer CalLab (a); In-house I-V measurements of the champion batch with a Sinton FCT-450 flash tester after calibration of the champion cell (red) by Fraunhofer ISE CalLab PV cells (b). (For interpretation of the references to color in this figure legend, the reader is referred to the web version of this article).

the Priority Academic Program Development of Jiangsu Higher Education Institutions.

References

[1] 〈http://pv.energytrend.com/research/PERC_Cells_Global_Production_Capacity_to_Reach_25GW_in_2017.html〉.

[2] 〈http://www.pv-tech.org/news/perc-solar-cell-migration-to-hit-25gw-in-2017-energytrend〉.

[3] Z. Liang, F. Zeng, H. Song, H. Shen, Effect of porous Si and an etch-back process on the performance of a selective emitter solar cell, Sol. Energy Mater. Sol. Cells 109 (2013) 26–32.

[4] G. Hahn, Status of selective emitter technology, in: Proceedings of the 25th EU PVSEC, Valencia, 2010, pp. 1091–1096.

[5] A. Zerga, A. Slaoui, J.C. Muller, B. Bazer-Bachi, D. Ballutaud, N. Le Quang, G. Goaer, SE formation for large scale industrially mc-Si solar cells by hydrogen plasma and wet etching, in: Proceedings of the 21st EC PVSEC, Dresden, 2006, pp. 865–869.

[6] H. Haverkamp, A. Dastgheib-Shirazi, B. Raabe, F. Book, G. Hahn, Minimizing the electrical losses on the front side: development of a selective emitter process from a single diffusion, in: Proceedings of the 33rd IEEE PVSC, San Diego, 2008, pp. 430–433.

[7] C. Dub, B. Tsefrekas Eacute, D. Buzby, R. Tavares, High efficiency selective emitter cells using patterned ion implantation, Energy Procedia 8 (4) (2011) 706–711.

[8] F. Book, A. Dastgheib-Shirazi, B. Raabe, H. Haverkamp, G. Hahn, P. Grabitz, Detailed analysis of high sheetresistance emitters for selectively doped silicon solar cells, in: Proceedings of the 24th EU PVSEC, Hamburg 2009, pp. 1719–1722.

[9] B. Tjahjono, J. Guo, Z. Hameiri, L. Mai, High efficiency solar cell structures through the use of laser doping, EUPVSEC (2007) 966–969.

[10] S. Lohmüller, E. Lohmüller, P. Saint-Cast, et al. Key Aspects for fabrication of p-Type Cz-Si PERC solar cells exceeding 22% conversion efficiency, in: Proceedings of hte 27th EUPVSEC, 2017, pp. 406-412.

[11] F. Ye, W. Deng, D. Chen, Y. Chen, The influence of a low doping concentration emitter on the performance of selective emitter silicon solar cells, in: Proceedings of the 24th EUPVSEC, 2014, pp. 1069-1071.

[12] Y. Komatsu, M.Koorn, et al. “Efficiency Improvement by Deeper Emitter with Lower Sheet Resistance forUniform Emitters” in: Proceedings of the 1st International Conference on Silicon Photovoltaics, 8, 2011, pp. 515–520.

[13] S. Werner, S. Mourad, et al., Structure and composition of phosphosilicate glass systems formed by POCl3 diffusion, Energy Procedia vol, (124) (2017) 455–463.

[14] P. Rothhardt et al. Control of phosphorus doping profiles for co-diffusion processes, in: Proceedings of the 27th EUPVSEC, 2012.

[15] H. Mäckel, K. Varner, On the determination of the emitter saturation current density from lifetime measurements of silicon devices, Prog. Photovolt. 21 (2013) 850–866.

[16] B. Min, A. Dastgheib-Shirazi, P. P. Altermatt, H. Kurz, “Accurate determination of the emitter saturation currentdensity for industrial P-diffused emitters”, in: Proceedings of the 29th EUPVEC, 2014, pp. 463-466.

[17] W. Deng, F. Ye, R. Liu, et al. 22.61% Efficient Fully Screen Printed PERC Solar Cell, in: Proceedings of the IEEE Photovoltaic Specialists Conference, 2017.

[18] R.A. Sinton, A. Cuevas, A quasi-steady-state open-circuit voltage method for solar cell characterization. in: Proceedings of the16th EUPVSEC,Vol, 2000, pp. 1152–1155.

[19] D.E. Kane, R.M. Swanson, Measurement of the emitter saturation current by a contactless photoconductivity decay method, in: Proceedings of the 18th IEEE Photovoltaic Specialists Conference, 1985, pp. 578–583.

[20] A. Kimmerle, J. Greulich, A. Wolf, Carrier-diffusion corrected J0-analysis of charge carrier lifetime measurements for increased consistency, Sol. Energy Mater. Sol. Cells 142 (2015) 116–122.

[21] A. Bentzen, A. Holt, J.S. Christensen, B.G. Svensson, High concentration in-diffusion of phosphorus in Si from a spray-on source, J. Appl. Phys. 99 (2006) 064502.

[22] J.W. Slotboom, H.C. De Graaff, Measurements of bandgap narrowing in Si bipolar transistors, Solid-State Electron. 19 (10) (1976) 857–862.

[23] M.S. Tyagi, R.V. Overstraeten, Minority carrier recombination in heavily-doped silicon, Solid-State Electron. 26 (6) (1983) 577–598.

[24] S.M. Sze, Physics of Semiconductor Devices, 2nd ed., John Wiley & Sons, New York, 1981.

[25] Y. Komatsu, G. Galbiati, M. Lamers, et al., Innovative diffusion processes for improved efficiency on industrialsolar cells by doping profile manipulation, in: Proceedings of the 24th EUPVSEC, 2009, pp.1063–7.

[26] R. McGill, J.W. Tukey, W.A. Larsen, Variations of box plots, Am. Stat. 32 (1978) 12–16.

[27] F. Ye, W. Deng, W.u. Guo, R. Liu, D. Chen, Y. Chen, Y. Yang, N. Yuan, J. Ding, Z. Feng, P. Altermatt, P. Verlinden, 22.13% Efficient Industrial P-Type Mono PERC Solar Cell, in: Proceedings of the 43rd IEEE PV Specialists Conference, 2016, pp. 3360–3365.